JES Focus Issue on Electrolysis for Increased Renewable Energy Penetration

Evaluation of MIEC $Ce_{0.8}Y_{0.1}Mn_{0.1}O_{2-\delta}$ Anode in Electrolyte-Supported SOFC

Hala T. Handal,[a,b,*] Paul Addo,[a,*] Aligul Buyukaksoy,[a] Viola Birss,[a,] and Venkataraman Thangadurai[a,***,z]**

[a]*Department of Chemistry, University of Calgary, Calgary, AB T2N 1N4, Canada*
[b]*Department of Chemistry, National Research Centre, Dokki, 12622 Cairo, Egypt*

In this study, the electrochemical performance of a single phase, mixed ion and electron conducting (MIEC) $Ce_{0.8}Y_{0.1}Mn_{0.1}O_{2-\delta}$ (10CYMO) anode was evaluated using symmetrical half-cell and full-cell configurations under humidified H_2, 10 ppm H_2S/H_2, and CH_4. An yttria-stabilized zirconia (YSZ) electrolyte support layer was used in this work, as ac impedance spectroscopy revealed that the 10CYMO/YSZ/10CYMO cell gave the lowest area specific polarization resistance (ASR) of 0.23 Ωcm^2 at 800°C in wet H_2, compared to $La_{0.8}Sr_{0.2}Ga_{0.8}Mg_{0.2}O_{3-\delta}$ (LSGM) and $Zr_{0.89}Sc_{0.1}Ce_{0.01}O_{2-\delta}$ (ScSZ). Exposure of the 10CYMO anodes to 10 ppm H_2S/H_2, either in a half-cell or full cell configuration, showed slight enhancement on the electrochemical performance, which was explained using a concept describing the sulfur and ceria interaction. The performance of a 10CYMO/YSZ/$La_{0.8}Sr_{0.2}MnO_{3-\delta}$ – YSZ full cell was evaluated under 90%H_2-N_2/3%H_2O, giving a power density of 75 mW/cm^2 at 800°C and is better than seen for other fluorite-based anodes reported in the literature.
© The Author(s) 2016. Published by ECS. This is an open access article distributed under the terms of the Creative Commons Attribution Non-Commercial No Derivatives 4.0 License (CC BY-NC-ND, http://creativecommons.org/licenses/by-nc-nd/4.0/), which permits non-commercial reuse, distribution, and reproduction in any medium, provided the original work is not changed in any way and is properly cited. For permission for commercial reuse, please email: oa@electrochem.org. [DOI: 10.1149/2.0121611jes] All rights reserved.

Manuscript submitted April 11, 2016; revised manuscript received June 6, 2016. Published June 28, 2016. *This paper is part of the JES Focus Issue on Electrolysis for Increased Renewable Energy Penetration.*

Nickel and yttria-stabilized zirconia (Ni-YSZ) composite materials are used as anodes in solid oxide fuel cells (SOFCs) because they meet most of the key requirements, such as a high electrical conductivity of $\sim 10^3$ Scm^{-1}, high catalytic activity for the hydrogen oxidation reaction (HOR), and thermal and chemical stability with YSZ at 700–1000°C.[1] Although the Ni-YSZ anode demonstrates good performance when H_2 is used as a fuel, this anode suffers from some drawbacks. These include a rapid deactivation of the Ni catalyst due to carbon deposition under hydrocarbon fuels.[2] Also, adsorption of sulfur species that are present in hydrocarbon fuels on the Ni surface results in its poisoning due to a decrease in the electrochemically active area for the HOR.[3] Furthermore, Ni coarsening[4] and redox instability[5] remain long-term issues in Ni-YSZ based SOFCs; therefore, immense work is in progress to find alternative anodes for advanced SOFCs.

Perovskite and fluorite-type metal oxides have shown several interesting functional properties toward sulfur tolerance and coking that make them promising anodes for SOFCs.[6] Acceptor-doped ceria exhibits mixed ion and electronic conduction (MIEC) in reducing conditions, which makes it suitable to be employed in anodes in intermediate temperature (IT) (500–750°C) SOFCs.[7] For example, Barnett et al.[8] showed that the addition of doped ceria to the Ni-YSZ anode resulted in a good SOFC performance with no deleterious coke formation at 600°C in wet CH_4. Nevertheless, the SOFC performance of doped ceria-based anodes in CH_4 was still significantly lower than in H_2.[9,10]

It is known that sulfur is present as H_2S in many common fuels and is added as an odorant in commercial fuels, such as natural gas. Thus, the stability of SOFC anodes toward sulfur poisoning is an important parameter, especially for the commercialization of SOFCs, operating on a variety of fuels.[3] Therefore, we have investigated the sulfur tolerance of ceria-based anodes, reporting that Ni infiltration into porous GDC yielded an anode that was stable in 10 ppm H_2S.[11] Also, B-site ordered double perovskite type tranisiton metals-doped $Ba_3CaNb_2O_9$ proved to be resistant to H_2S poisoning when it was examined under a high concentration of H_2S (5000 ppm).[12] Although good chemical stability was achieved with these anode materials, the electrochemical performance has remained unsatisfactory.[11,12]

Recently,[13] using a symmetrical half-cell, we obtained a promisingly low polarization resistance (Rp) value of 0.3 Ωcm^2 at 800°C with a $Ce_{0.9}Y_{0.1}O_{2-\delta}$ (CYO) anode in humidified H_2. Also, $Ce_{0.9}Y_{0.1}Mn_{0.1}O_{2-\delta}$ (10CYMO) showed high electrical conductivity under H_2 (0.15 Scm^{-1} at 700°C) with improved sulfur tolerance as compared to that of Mn-free CYO. The electrical conductivity of CYO lies within the range of the values measured for some known MIECs (mixed ion and electron conductors), such as $LaSrFeO_4$-based anodes.[14] In spite of their lower electrical conductivities as compared to Ni-YSZ, these anodes exhibit superior chemical stability under H_2S. This encouraged us to evaluate the electrochemical performance of the fluorite-based anode 10CYMO using both symmetrical half-cell and full cell configurations in humidified H_2, with or without the addition of ppm levels of H_2S and also in wet CH_4 fuels.

Experimental

Button cell fabrication.—A metal oxide of nominal composition $Ce_{0.8}Y_{0.1}Mn_{0.1}O_{2-\delta}$ (10CYMO) was prepared using the citric acid auto-combustion method.[13] For electrical conductivity measurements, part of the powder was pelletized and sintered at 1350°C in air. Au paste was brush-painted on each side of the pellet to serve as current collectors, and then heated at 800°C for 15 mins (Heraeus Inc., LP A88-11S, Germany).

For the fuel study, three different oxide ion electrolytes, including $La_{0.8}Sr_{0.2}Ga_{0.8}Mg_{0.2}O_{3-\delta}$ (LSGM) (Fuel Cell Material (USA)), $Zr_{0.89}Sc_{0.1}Ce_{0.01}O_{2-\delta}$ (ScSZ) (PRAXAIR (99.9%, Canada)) and $Zr_{0.84}Y_{0.16}O_{2-\delta}$ (YSZ) (TOSOH (Tosoh-8Y, Japan)) were prepared by the sintering of pellets of powders. The YSZ and ScSZ pellets were sintered at 1400°C, while the LSGM pellets were sintered at 1350°C for 24 h. Calcined 10CYMO powder was then mixed with a homemade organic slurry to prepare the anode ink, which was deposited onto the two sides of the LSGM (2.5 mm thick disc), ScSZ (2.6 mm thick disc) and YSZ (0.8 mm thick disc) electrolytes to fabricate symmetrical half-cells. To fabricate the full cell, 10CYMO was deposited only on one side of the YSZ electrolyte (1.2 mm thick disc) to form the anode layer (~16–20 μm thick). The deposited layers were annealed prior to measurements at 1000°C for 5 hours. Further details

*Electrochemical Society Student Member.
**Electrochemical Society Fellow.
***Electrochemical Society Member.
[z]E-mail: vthangad@ucalgary.ca

Downloaded on 2016-08-30 to IP 136.159.160.69 address. Redistribution subject to ECS terms of use (see ecsdl.org/site/terms_use) unless CC License in place (see abstract).

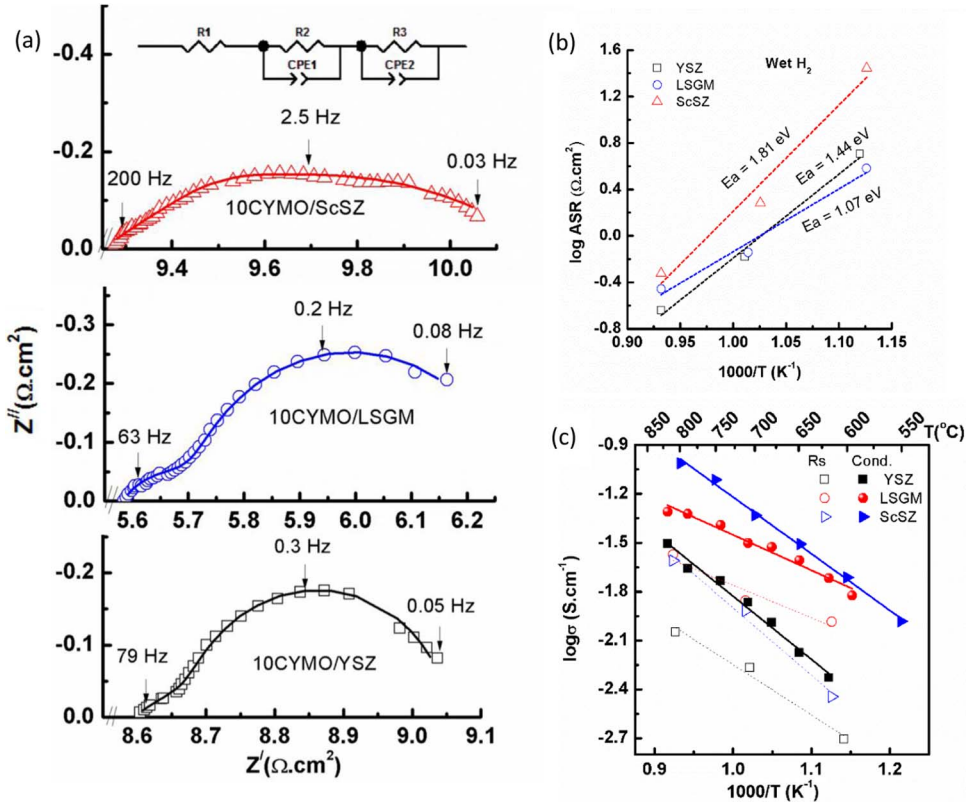

Figure 1. (a) Impedance spectra of the configuration 10CYMO/electrolyte/10CYMO measured at 800°C in 3%H_2O/H_2 at OCV, (b) log ASR vs 1/T, (c) The conductivity as a function of temperature for the aforementioned electrolytes with 10CYMO electrode (open symbol) and without (closed symbol). Au was used as a current collector in both cases.

about the procedure for the symmetrical half-cell preparation have been reported elsewhere.[13]

To form the cathode for the full cell studies, a polymeric $La_{0.8}Sr_{0.2}MnO_{3-\delta}$ (LSM) precursor was infiltrated into a porous YSZ scaffold (≈10 μm thick), produced using methods developed earlier.[15] LSM was synthesized by dissolving appropriate amounts of $La(NO_3)_3.6H_2O$, $Sr(NO_3)_2.xH_2O$ and $Mn(NO_3)_2.xH_2O$ (Alfa Aesar, purity >90%) in water, followed by the addition of ethylene glycol so that the molar ratio of ethylene glycol to the cations is 0.04. The mixture was continuously stirred at 80°C until complete water removal was achieved and then 2-butoxyethanol was added at the end to enhance the wettability of the solution.[15] The precursor solution was infiltrated into the porous YSZ layer and then decomposed at 400°C, with these infiltration/decomposition cycles repeated 20 times. In order to evaluate the cathode performance free from the anode contribution, symmetrical half-cells with infiltrated LSM-YSZ cathodes on both sides of a YSZ disc electrolyte (~0.19 cm thick) were prepared separately. Au paste was painted on both sides of the button cells to serve as current collectors.

Electrochemical characterization.—The electrochemical performance of the 10CYMO was tested by loading the fabricated button cell in a FCSH-V3 cell holder (Materials Mate, Italy). A glass sealant (Type 613, Aremco Products, USA) was used to ensure separation of the anode (fuel) and cathode (air) gases. Fuels having a composition of 3%H_2O/H_2, 10–90% H_2 -N_2/3%H_2O, 10 ppm H_2S/50%H_2-N_2/3%H_2O, 3%H_2O/CH_4, and 90%CH_4-N_2/3%H_2O were introduced to the anode side of the full cell and half cell with a flow rate 25 sccm, while the cathode was exposed to air in full cell operation. The *V-I* characteristics and ac impedance response were measured for the full cell at 800°C using a four-probe method. Impedance spectra were collected under OCV (open circuit voltage) using a RMS amplitude of 50 mV in the frequency range of 0.01 Hz–60 kHz (Solatron1287/1255 potentiostat/galvanostatic impedance analyzer).

Chronoamperometry experiments were carried out for symmetrical anode half-cells using VersaStat3 potentiostatic/galvanostatic (METEK) instrument to study the effect of 10 ppm H_2S in H_2 on the cell performance by applying a 100 mV constant potential at 800°C. Electrical conductivity measurements were performed on sintered pellets using AC impedance spectroscopy (Solartron Electrochemical Impedance Spectroscopy; EIS model 1260, 100 mV; 0.01 Hz–1 MHz) in the temperature range of 300–800°C in H_2/3%H_2O and 30 ppm H_2S/H_2. Electrochemical impedance spectroscopy was used to determine the area specific polarization resistance (ASR) of the 10CYMO anode and infiltrated LSM-YSZ cathode half-cells at the OCV in air and in wet H_2 using ac amplitude of 100 mV at 600–800°C. The chemical reactivity between the 10CYMO anode and the YSZ electrolyte was investigated in a symmetrical cell configuration using scanning electron microscopy (SEM) and line scan energy dispersive X-ray analysis, EDX (SEM, Model JSM-6400, JEOL Corporation, Japan).

Results and Discussion

Compatibility studies of 10CYMO with various electrolytes using ac-impedance.—Figure 1a shows the typical impedance plots of a symmetrical half-cell with a 10CYMO anode, employing several oxide ion conducting ceramic electrolytes, all at 800°C in H_2/3%H_2O. The Nyquist plots can be fitted using an equivalent circuit consisting of a resistor (Rs) in series with two other resistors, each connected in parallel to constant phase elements (R1-CPE1 and R2-CPE2). Rs represents an ohmic resistor dominated by the solid electrolyte resistance, R1-CPE1 defines the high-frequency process, and R2-CPE2 defines the low-frequency process (Figure 1a inset). While Gerischer and/or Warburg elements were initially used to fit the impedance data, as suggested by Holtappels et al.,[16] the best fit was obtained using the two R-CPE circuit (Fig. 1a), as reported by others.[17]

The full diameter of the two semi-circles refers to the total polarization resistance (Rp). In the case of a symmetrical half-cell, the

Downloaded on 2016-08-30 to IP 136.159.160.69 address. Redistribution subject to ECS terms of use (see ecsdl.org/site/terms_use) unless CC License in place (see abstract).

electrode impedance (Rp) should be divided by 2 to obtain an area specific polarization resistance (ASR). The impedance spectra collected from symmetrical half- cells with YSZ and LSGM as the electrolyte were quite similar in shape. The lowest ASR of 0.23 Ωcm^2 at 800°C in wet H_2 was obtained for the 10CYMO/YSZ/10CYMO cell, while the ASR values obtained from the symmetrical half-cell with LSGM and ScSZ as the electrolytes were 0.35 Ωcm^2 and 0.47 Ωcm^2, respectively, under the same conditions.

It should be noted that the ac impedance data are dominated by the low-frequency process in all cases, showing a summit frequency in the range of 0.2 to 2.5 Hz. In order to understand the nature of the dominant low-frequency arc, a temperature dependence ASR study was carried out. The low- frequency arc observed in Figure 1b decreased significantly with temperature, indicating a thermally activated process, excluding the possibility of gas diffusion impedance. Relatively high activation energy (E_a) values were obtained for the three half-cell configurations (1.07–1.81 eV) and the capacitance values calculated from the impedance fittings for the low-frequency process was in the range of 0.1–10 Fcm^{-2}.

The low-frequency arc can be assigned to a chemical capacitance, as reported for many other MIECs.[18,19] The chemical capacitance for porous ceria films was reported to be 0.021–0.32 Fcm^{-2}, which is assumed to originate from changes in the oxygen stoichiometry.[20] It is known that the incorporation or expulsion of oxide ions is driven by a change in the oxidation states of the host cations in the bulk, which leads to a large chemical capacitance (pseudo-capacitance), approaching 1 Fcm^{-2} or larger.[20] We believe that the reduction of Ce^{4+} in the low pO_2 environment of the anode would result in the accumulation of oxide ion vacancies and electrons (Ce^{3+}) in the bulk of the electrodes. A chemical capacitance for SDC thin films was reported to be in the range of 0.14–1.56 Fcm^{-2}.[17]

In order to determine whether any additional resistance is introduced upon the deposition and annealing of the 10CYMO electrode on the oxide ion conducting electrolytes, the electrical conductivity of the electrolytes was calculated from the series resistance (Rs) of the symmetrical half-cells and compared to those of the as-prepared electrolytes with Au current collectors (Figure 1c). The as-prepared ScSZ, LSGM, and YSZ electrolyte conductivity at 800°C in H_2 was found to be 0.098 Scm^{-1}, 0.049 Scm^{-1} and 0.031 Scm^{-1}, respectively. The estimated conductivities from the symmetrical half-cell measurements in H_2/3%H_2O were 0.028 Scm^{-1}, 0.045 Scm^{-1} and 0.009 Scm^{-1} at 800°C for ScSZ, LSGM and YSZ, respectively.

The ohmic resistance of LSGM appears to be the least affected by the addition of the 10CYMO (ca. 8% drop in the conductivity). Chemical compatibility studies (not shown here), carried out using PXRD revealed the dissolution of Ce from 10CYMO into the ScSZ electrolyte during the co-firing process of 10CYMO and ScSZ electrolyte. However, no other by-product was seen in the case of either the LSGM or YSZ electrolytes. In the case of LSGM, it was anticipated that diffusion of La into the 10CYMO electrode may occur, affecting the oxygen stoichiometry inside the 10CYMO electrode layer and stabilizing it against reduction under the low pO_2 environment of the anode and eventually affecting the ASR in H_2/3%H_2O.[21] This factor may rationalize the higher ASR seen for the symmetrical cell based on the LSGM electrolyte compared to YSZ (Figure 1a). However, the minor change in the ohmic resistance of the LSGM electrolyte, determined from the symmetrical cell versus from the as-prepared LSGM conductivity, could arise from substantial differences in the thickness of the LSGM and 10CYMO electrode layers. Also, La diffusion at LSGM/10CYMO interface seems to affect only the electrode with a minor influence on the LSGM electrolyte (Figure 1c).

To establish the chemical stability of the 10CYMO/YSZ interface, a cross-section of a half-cell with a 10CYMO/YSZ/10CYMO configuration was examined using SEM and EDX (Figure 2). The EDX line-scan shows a drop in the Ce concentration at the YSZ electrolyte/10CYMO electrode interface. Ce-doped YSZ, $Zr_{0.84-x}Ce_xY_{0.16}O_{2-\delta}$, exhibits the low oxide ion conductivity compared to the YSZ electrolyte.[22] Despite the possibility of an interfacial chemical reaction between 10CYMO and the YSZ electrolyte, the lowest ASR was observed in the half-cell with the YSZ electrolyte. Therefore, the remainder of this study was performed using the YSZ electrolyte.

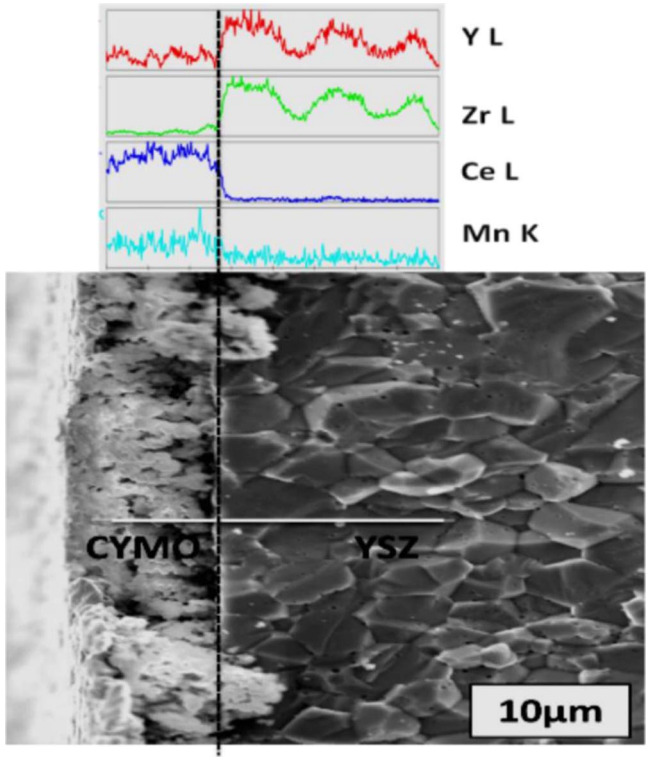

Figure 2. Selected area SEM image of the electrolyte supported symmetrical cell with YSZ (2.09 mm thick YSZ) and 10CYMO. The top scheme represents the line scanning EDX across the electrode /electrolyte interface.

Symmetrical half-cell studies involving 10CYMO anodes in H_2 and in low ppm H_2S.—To further understand the nature of the processes that take place at the 10CYMO anode on YSZ electrolytes, impedance measurements were performed at different H_2 partial pressures (pH_2) (Figure 3). The low- frequency arc shifts to lower Z-values as the pH_2 increases, while the high-frequency arc is found to be

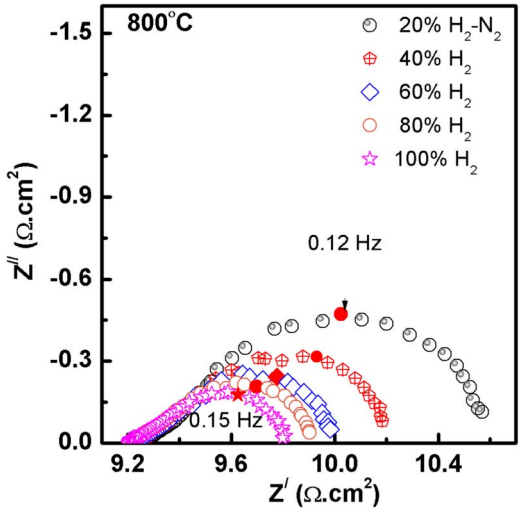

Figure 3. Impedance spectra of the electrolyte-supported symmetrical cell 10CYMO/YSZ/10CYMO measured at 800°C in different concentration of humidified H_2 at OCV.

Downloaded on 2016-08-30 to IP 136.159.160.69 address. Redistribution subject to ECS terms of use (see ecsdl.org/site/terms_use) unless CC License in place (see abstract).

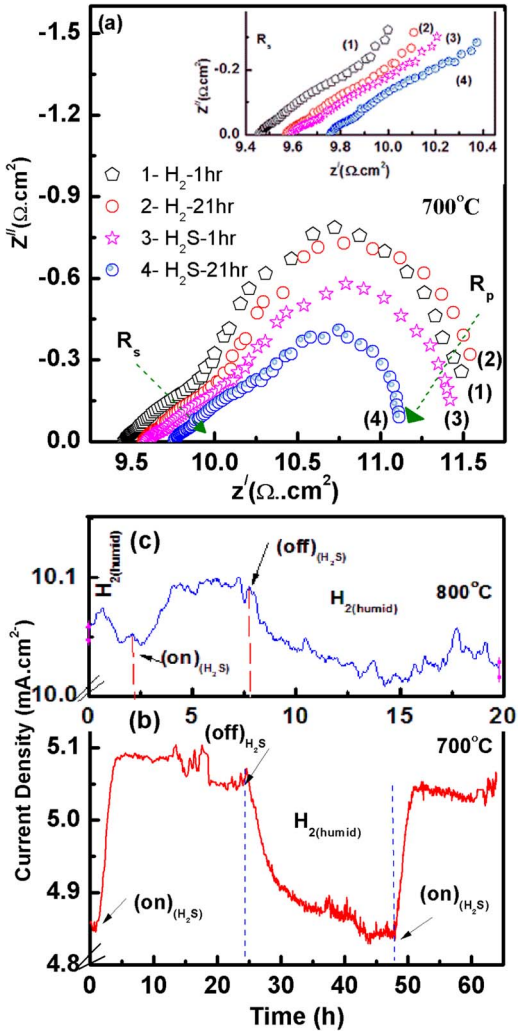

Figure 4. (a) Impedance plot of 10CYMO/YSZ/10CYMO measured under a mixture of humidified H_2 and H_2 containing 10 ppm H_2S at OCV and 700°C. The current density as a function of time for the symmetrical cell at (b) 700°C and (c) 800°C, respectively. The cell was kept at 100 mV and was running on 10 ppm $H_2S/H_2/3\%H_2O$.

slightly changed. Increasing pH_2 tends to increase the concentration of Ce^{3+}, leading to improved electronic conduction in 10CYMO. Thus, the electrochemical reaction will not be limited to the triple-phase-boundary (TPB). Instead, it will extend to the entire active surface of the 10CYMO, as reported by the Haile group.[23] A similar shrinkage in the low-frequency resistance with increasing pH_2 was also observed by Decaluwea et al.,[24] who attributed it to enhanced oxide ion diffusion in CeO_2.

Figure 4a shows the effect of H_2S on the electrochemical performance of the symmetrical cell. There are two main observations: (i) the low-frequency arc shrinks upon adding H_2S and (ii) switching from H_2 to H_2S results in a slight increase in Rs. The calculated capacitance value for the low-frequency arc after 21 hours exposure to H_2 was 2.3 Fcm^{-2}, which increased to 2.8 Fcm^{-2} upon exposure to 10 ppm H_2S/H_2. This change suggests that H_2S incorporation into the ceria matrix plays a role in its reduction, increasing both the Ce^{3+} and oxide ion vacancy concentration. Figures 4b and 4c show the chronoamperometry data for the YSZ-supported cell with 10CYMO electrodes attached to both sides of the electrolyte at 700°C and 800°C, respectively. An enhancement in the current density and in the stability of the performance was observed upon exposure to 10 ppm H_2S/H_2. The thick disk of YSZ (1 mm) is the main reason for the very large ohmic drop, and considering how much thinner the electrode layer

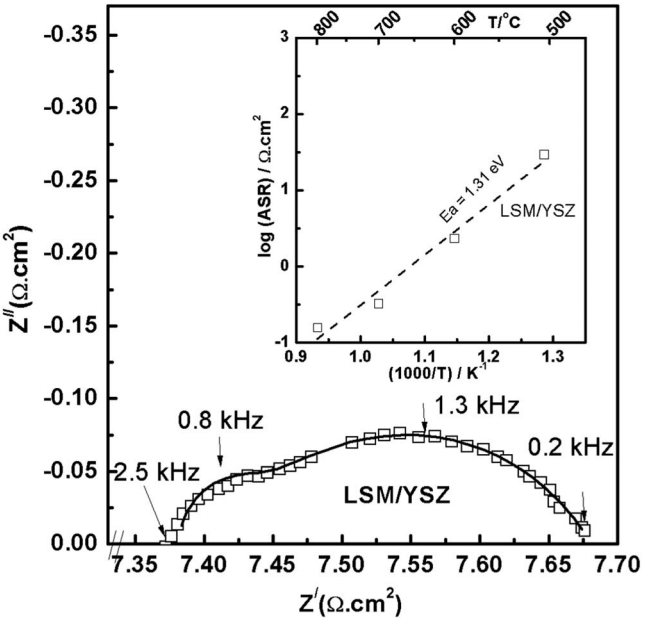

Figure 5. Typical impedance plot of symmetrical cell cathode of the LSM infiltrated YSZ on the top of YSZ electrolyte that was measured at 800°C. The inset figure represents the ASR as a function of temperature.

is (~16 μm), the change in the current density under these two conditions is considered to be significant. At 700°C, the recovery in the performance of the anode layer is close to 100%, and the equilibration time is fairly long upon switching the gas from 10 ppm H_2S/H_2 to H_2. The phase diagram of the Ce-O-S system at 800°C predicts the possibility of the formation of Ce_2O_2S under high reducing conditions and at high concentrations of H_2S. Thus, it is unlikely that bulk cerium sulfide would be under the present experimental conditions.[25]

Full-cell evaluation of YSZ-supported cell with 10CYMO electrodes.—To further evaluate the 10CYMO anode performance, full-cell measurements in H_2 and also in H_2/H_2S were made, using LSM-YSZ cathodes. To determine the LSM-YSZ composite cathode activity, it was investigated first in a symmetrical half-cell prior to the full-cell test. Figure 5 shows the typical impedance spectrum for LSM-YSZ composite electrodes placed on both sides of a YSZ electrolyte. An ASR of 0.15 Ωcm^2 at 800°C in air is seen, with a summit frequency of ~1 kHz. The ASR observed for this material is comparable to other types of fluorite-type anodes reported previously.[9,26] For example, Fuerte et al.[9] showed a total ASR of 2.11 Ωcm^2 for a Cu-ceria based anode under H_2/N_2 at 750°C. The inset in Figure 5 shows the temperature dependence of the ASR of the LSM-YSZ cathode, giving an activation energy of 1.3 eV, which matches the reported values for LSM-YSZ composite cathodes.[16] Comparing the ASR of the 10CYMO (Figure 1) with that for LSM-YSZ (Figure 5), oxygen reduction at LSM-YSZ is not expected to be the rate limiting reaction in a 10CYMO/YSZ/LSM-YSZ cell at 500–800°C.

Figure 6 shows the impedance spectra and V-I curves of the full cell with the configuration 10CYMO/YSZ/LSM-YSZ in $50\%H_2$-$N_2/3\%H_2O$ (with and without the addition of 10 ppm H_2S) as the fuel and air as the oxidant, all at 800°C. The Nyquist plot in Figure 6a shows an ASR of ca. 1.4 Ωcm^2 in 50% H_2-$N_2/3\%H_2O$ at 800°C, with a slight decrease in its value when 10 ppm H_2S was added. This further confirms the half-cell studies that showed that the activity of the 10CYMO anode toward the HOR is enhanced in the presence of a few ppm H_2S.

Figure 6b shows the performance plot of the cell in H_2/N_2, with and without the addition of 10 ppm H_2S, at 800°C. The cell showed a maximum current density of 150 $mAcm^{-2}$ and a power density of 75 mW/cm^2. The performance is slightly better than seen for other

Downloaded on 2016-08-30 to IP 136.159.160.69 address. Redistribution subject to ECS terms of use (see ecsdl.org/site/terms_use) unless CC License in place (see abstract).

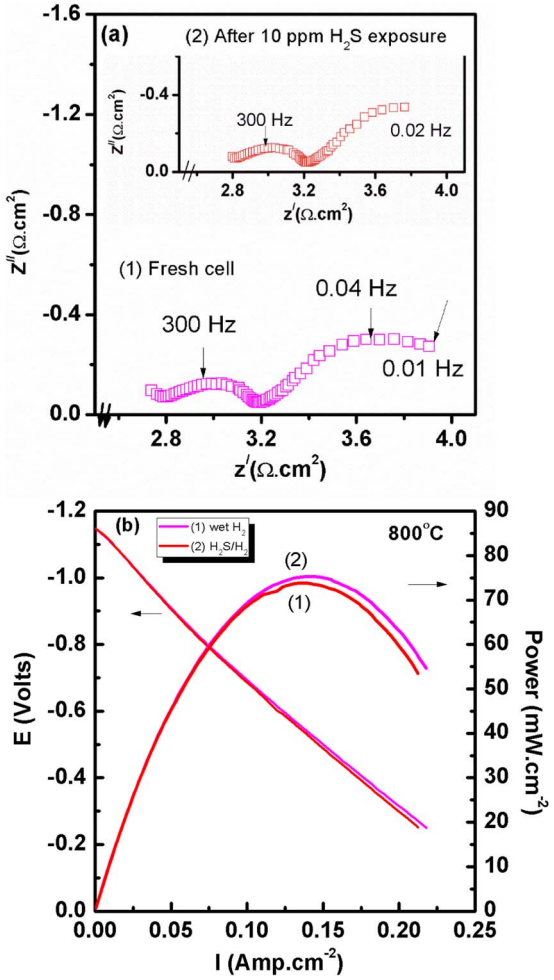

Figure 6. Electrochemical performance of (a) impedance and (b) V-I plot of 10CYMO (anode)/YSZ/LSM-YSZ (cathode) single full cell measured under 50% H_2-N_2 (3%H_2O), and 10ppm H_2S in 50% H_2-N_2 (3%H_2O) as a fuel and air as an oxidant at 800°C. The inset figure in (a) is the cell performance after exposure to 10 ppm H_2S-H_2.

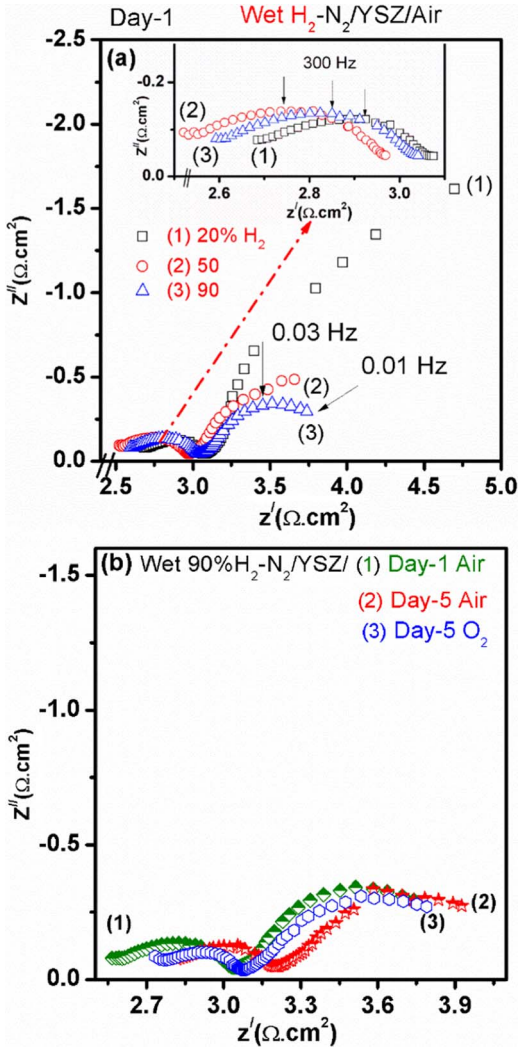

Figure 7. Electrochemical performance of the single button cell of the configuration: 10CYMO (anode)/YSZ/LSM-YSZ (infiltrated cathode) presented by Nyquist plots measured under different (a) hydrogen and (b) oxygen concentrations at 800°C. Also, figure b displays the impedance spectra collected for the single cell in day 1 versus day 5.

fluorite-based anodes that do not also contain metal catalysts, such as Ru and Ni.[27] The relatively low power density seen here can be attributed to the fact that a thick electrolyte was used in our work, therefore leading to a higher ohmic resistance.

To determine the individual contributions of the anode and cathode to the polarization resistance, the anode was fed with various pH_2 (Figure 7a) and the cathode was switched from air to pure O_2 (Figure 7b). It can be seen that the high-frequency arc decreases with increasing pO_2 (Figure 7a). By fitting the Nyquist plot to an equivalent circuit [(Rs)(R1/CPE1) (R2/CPE2)], the total R_p due to the sum of the high (R1) and low-frequency arcs (R2) were found to decrease from (0.27 (R1)+1.91 (R2)) Ωcm^2 in 20% H_2 to (0.30 (R1) + 0.69 (R2)) Ωcm^2 in 50% H_2 and (0.26 (R1) + 0.55 (R2)) Ωcm^2 in 90% H_2 at 800°C. It was observed that the H_2 content influenced only the low-frequency resistance (R2), while the high-frequency resistance (R1) remained almost unchanged (Figure 7). This means that the low-frequency arc is due to the HOR process occurring at the anode side, while the high-frequency arc can be attributed to the ORR at the cathode side. The series resistance decreased from 2.18 Ωcm^2 in 10% H_2 to 2.13 Ωcm^2 in 90% H_2. This is not surprising because, as the H_2 content is increased, the 10CYMO electrode becomes more reduced, leading to an increase in the total electrical conductivity (Figure 3). Furthermore, Figure 7b shows that the 10CYMO electrode had a stable electrochemical performance after 5 days in H_2 at 800°C.

Effect of H_2S on the electrical properties of the 10CYMO.— In order to understand the stable (and even improved) performance of 10CYMO with exposure to a few ppm H_2S, the interaction of H_2S with the 10CYMO anode material in pellet form was further investigated by monitoring its impact on the electrical conductivity. Figure 8 shows the electrical conductivity of the 10CYMO pellet, before and after exposure to 30 ppm H_2S in H_2. An enhancement in the conductivity was observed upon changing the atmosphere from air to H_2, with almost no change seen in the activation energy (ca. 1 eV). However, a significant drop in the activation energy accompanied switching the gas from H_2 to 30 ppm H_2S/H_2, from 1 eV to 0.47 eV. Measuring the conductivity after re-oxidation of the sample in air at 700°C overnight showed an order of magnitude decline in the conductivity compared to the as-prepared sample, while the activation energy was found to be 0.9 eV. A second exposure of the sample to 30 ppm H_2S/H_2 displayed an enhancement in the conductivity, although lower conductivity values were observed as compared to after the first exposure to H_2S. The activation energy remained the same as what was observed upon exposure to H_2S the first time (0.47 eV). The activation energies for the samples measured in air, after exposed to H_2S, are consistent with oxide ion mobility.[28] However, the activation energy of the re-oxidized sample (0.9 eV) was found to be closer

Downloaded on 2016-08-30 to IP 136.159.160.69 address. Redistribution subject to ECS terms of use (see ecsdl.org/site/terms_use) unless CC License in place (see abstract).

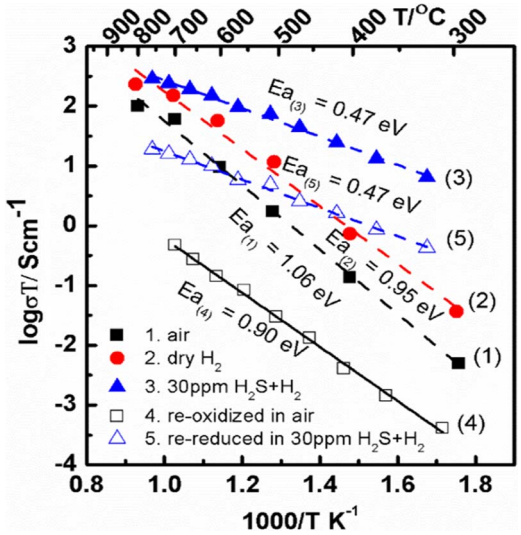

Figure 8. Comparison of the total electrical conductivity of 10CYMO measured in (1) ambient air, (2) dry H_2, (3) dry H_2 with 30ppm H_2S, (4) ambient air after re-oxidized sample in 3 in air at 700°C/12 h and (5) dry H_2 with 30 ppm H_2S after re-reduced sample in 4 in the aforementioned gas at 700°C/12 h.

to the activation energy of the reduced sample (0.95 eV). Changes in the microstructure, the defect types and their concentrations are apparently the main reasons for the difference in activation energy between the highly oxidized as-prepared sample and the re-oxidized one. Further work is required to fully understand the effect of sample thermal history on electrical conductivity.

In our earlier work,[29] we did not detect any impurity phases (for e.g., MnS or CeO_2S_2) in the 10CYMO powder exposed for 24 h to 30 ppm H_2S/H_2 at 800°C, even though SEM and EDX analysis confirmed the presence of sulfur. Figure 8 showed that the same activation energy was seen for samples exposed to H_2S/H_2 as in H_2 alone, indicating that the same mechanism of conduction prevails. The enhancement of the conductivity upon H_2S exposure may be explained as follows. In the first step, H_2S dissociates into H_2 and S on the surface of doped ceria. Subsequently, S may interact with the lattice oxygen at the surface, forming oxides that may be desorbed at the measurement temperature with a continuous replenishment of the oxide ion species by the ones diffuse from the bulk. Over a prolonged exposure to 30 ppm H_2S in a reducing atmosphere, sulfur may occupy the oxide ion vacancies and the accumulation of sulfur in the bulk of the oxygen-deficient phase is expected, introducing a new donor level in the bandgap of ceria, thus lowering the energy required for electronic transitions. Kobayashi and coworker[30] showed that there is a tendency for ceria to undergo sulfidation, enhancing its reducibility under low pO_2 condition. This sulfur uptake is manifested in the enhancement of the electrical conductivity and the decline in activation energy of the 10CYMO samples that were exposed to 30 ppm H_2S. The potential formation of electronic conducting Ce_2S_3 could also be the reason for the enhancement in electrical conductivity.[31] However, this prediction could not be verified by room-temperature PXRD analysis. Upon cooling the system, the pO_2 will increase and surface sulfur seems to be desorbed, while bulk sulfur is expected to remain in the sample.[29]

It has been reported that MIECs are more sulfur tolerant than cermets.[3] However, the mechanism for resisting sulfur poisoning has not been clearly explained, as yet. In addition, the impact of the operating temperature, which is of equal importance to the H_2S concentration in affecting the type of sulfur species present, has rarely been taken into consideration. At a fixed temperature, the amount of transition metal present in the anode, whether it is an MIEC or a cermet, seems to control the extent of S poisoning. As the transition metal concentration increases, the stability of the MIEC declines and a metal sulfide can be detected, as seen in earlier work.[32] Transition metal oxides, including FeO, MnO, CuO, and ZnO, are good sorbents for sulfur and are used for de-sulfurization in coal gasification systems at high temperatures and at low pO_2.[33] MnO was seen to be superior to other oxides because of its low tendency to reduce to the metallic state under reducing conditions. Accordingly, it can be suggested that the tolerance of ceria toward sulfur seems to be partially the result of the presence of the reduced ceria phase (Y-doped CeO_2 (CYO) is known for its tendency to interact with sulfur under reducing conditions), but also due to the addition of Mn. The generation of sulfur-free ceria and Mn under oxidizing conditions was previously reported[34] upon lowering the temperature and increasing the pO_2. In air, any accumulated sulfur on the surface of a 10CYMO pellet is predicted to desorb in the form of SO_x, while some cerium sulfate may remain after re-oxidation at 700°C, as reported elsewhere.[35] To verify these assumptions and further understand the interaction of H_2S on 10 CYMO, there is need to employ some form of in-situ technique such as Raman spectroscopy, which has been used to characterize the interaction of H_2S especially on Ni -based SOFC anodes.[36,37]

Full Cell Performance of 10CYMO anode in hydrocarbon fuels.—In order to evaluate the feasibility of using 10CYMO in hydrocarbon fuels, the full cell performance was investigated using wet CH_4. The impedance spectra of the CYMO/YSZ/ LSM/YSZ cell show a total polarization resistance of 23.3 Ωcm^2 and an ohmic resistance of 1.7 Ωcm^2 at 800°C (Figure 9a), which is in the range reported by Stomer et al.[38] for a GDC/YSZ/GDC cell (ASR of 30 Ωcm^2 at 700°C).

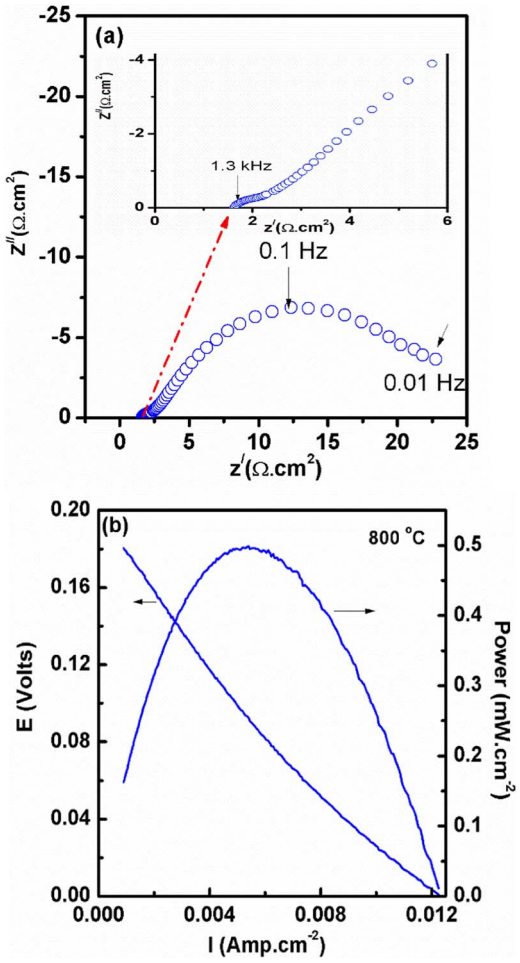

Figure 9. Electrochemical performance of (a) impedance and (b) V-I curve of 10CYMO (anode)/YSZ/LSM-YSZ) (cathode) single cell measured under 90% humidified CH_4/N_2 as a fuel and air as an oxidant at 800°C. The inset figure in (a) is the magnified part of Nyquist plot at high frequency.

Downloaded on 2016-08-30 to IP 136.159.160.69 address. Redistribution subject to ECS terms of use (see ecsdl.org/site/terms_use) unless CC License in place (see abstract).

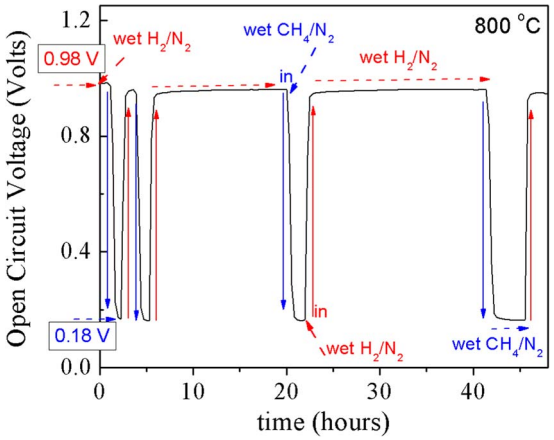

Figure 10. The change of OCV as a function of time measured for a single button cell upon switching the gas between H_2/wet N_2 into CH_4/wet N_2.

However, a very low OCV of ca. 200 mV and a very poor maximum power density of only ca. 0.5 mWcm^{-2} were observed (Figure 9b).

The poor performance of the full cell under methane (Figure 9) is not surprising, considering the very low electronic conductivity of the 10CYMO anode. A fast drop in the OCV to 200 mV upon exposure of the system to wet CH_4 is consistent with the work of Putna et al.[27] Marina and Mogensen[39] also studied the performance of a $Ce_{0.6}Gd_{0.4}O_{1.8}$ (CGO) anode for the electrochemical oxidation of CH_4 at 1000°C. While their measured OCV was 730 mV, they associated this still relatively low OCV to the poor catalytic activity of the CGO anode to CH_4 oxidation. Also, the low OCV was attributed to the low pH_2 that is thermally produced at the anode side.[39]

However, the drop in the OCV in the present study is more substantial than reported by Marina and Mogensen,[39] perhaps related to the lower operating temperature and the higher CH_4 partial pressure. To determine if this OCV behavior was related to poor sealing of the cell, we measured the changes in the OCV as a function of time of switching the anode gas between wet H_2 and CH_4 at 800°C (Figure 10). The OCV recorded in 3%H_2O/H_2 was 0.98 V vs. air, but dropped abruptly to 0.18 V vs. air upon switching to 3%H_2O/CH_4. This behavior was reproducible, based on the four cycles between 3%H_2O/H_2 and 3%H_2O/CH_4. Therefore, the possibility of gas leakage due to poor sealing can be eliminated. Further experimental and or theoretical studies are required to elucidate the unexpectedly poor performance observed when the 10CYMO anode was operated under 3%H_2O/CH_4 in a full cell configuration.

Conclusions

Under the investigated conditions, single phase, mixed conducting 10CYMO ceria anodes showed a better performance when using a YSZ electrolyte support, compared to LSGM and ScSZ. The power output for a full cell based on a 10CYMO anode, a YSZ electrolyte, and a LSM infiltrated YSZ cathode was 75 mW/cm^2 at 800°C. The losses were due primarily to the electrolyte resistance and the anode polarization. Analysis of the impedance response in humidified H_2 showed that the chemical capacitance of the anode dominated at low frequencies, while the cathode response appeared at a high frequencies. Both half cell and full cell performances improved slightly with exposure to 10 ppm H_2S at 800°C. Conductivity measurements were employed to understand the synergistic effect between H_2S and ceria. Complete full cell performance measurements under wet CH_4 suggest a poor catalytic activity of 10CYMO toward CH_4 oxidation.

Acknowledgments

We thank the Natural Sciences and Engineering Research Council of Canada (NSERC) for funding through Discovery Grants (DG), and Research Tools and Instruments infrastructure grants (RTI) (cat. 1), and the Canada Foundation for Innovation (CFI) awards. We also thank Dr. Anand Singh, Department of Chemistry, University of Calgary for his help with the SOFC measurements. H.H. gratefully acknowledges the Arab Republic of Egypt Fellowship program, A.B. extends his thanks to the Eyes High PDF Program at the University of Calgary and Alberta Innovates -Technology Futures (AITF) for their financial support, and P.A. acknowledges AITF for scholarship support. We also thank Prof. Kim Hea Bok and Dr. ZhaoKai from the Department of Hydrogen and Fuel Cells Engineering, Chonbuk National University, South Korea, for the SEM/EDX measurements.

References

1. Z. Cheng, J.-H. Wang, Y. Choi, L. Yang, M. C. Lin, and M. Liu. , "From Ni-YSZ to sulfur-tolerant anode materials for SOFCs: electrochemical behavior, in situ characterization, modeling, and future perspectives," *Energy Environ. Sci.*, **4**, 4380 (2011).
2. C. H. Bartholomew, "Carbon deposition in steam reforming and methanation," *Cat. Rev.*, **24**, 67 (1982).
3. M. Gong, X. Liu, J. Trembly, and C. Johnson, "Sulfur-tolerant anode materials for solid oxide fuel cell application," *J. Power Sources*, **168**, 289 (2007).
4. B. Iwanschitz, L. Holzer, A. Mai, and M. Schütze, "Nickel agglomeration in solid oxide fuel cells: The influence of temperature," *Solid State Ionics*, **211**, 69 (2012).
5. D. A. Sarantaridis, "Redox cycling of Ni-Based solid oxide fuel cell anodes: a review," *Fuel Cells*, **7**, 246 (2007).
6. S. P. S. Shaikh A. Muchtar and M. R. Somalu, "A review on the selection of anode materials for solid-oxide fuel cells," *Renew. Sustainable Energy Rev.*, **51**, 1 (2015).
7. E. H. Baker, M. Iqbal, and B. E. Knox, "Conductivity measurements on ceria at high oxygen pressures," *J. Mater. Sci.*, **12**, 305 (1977).
8. E. P. Murray, T. Tsai, and S. A. Barnett, "A direct-methane fuel cell with a ceria-based anode," *Nat.*, **400**, 649 (1999).
9. A. Fuerte, R. X. Valenzuela, M. J. Escudero, and L. Daza, "Effect of cobalt incorporation in copper-ceria based anodes for hydrocarbon utilisation in intermediate temperature solid oxide fuel cells," *J. Power Sources*, **196**, 4324 (2011).
10. M. D. Gross, J. M. Vohs, and R. J. Gorte, "An examination of SOFC anode functional layers based on ceria in YSZ," *J. Electrochem. Soc.*, **154**, B694 (2007).
11. B. Mirfakhraei, S. Paulson, V. Thangadurai, and V. Birss, "Enhanced hydrogen oxidation activity and H_2S tolerance of Ni-infiltrated ceria solid oxide fuel cell anodes," *J. Power Sources*, **243**, 95 (2013).
12. W. H. Kan, M. Roushanafshar, A. Vincent, T. Furstenhaupt, M. Parvez, J. Lu, and V. Thangadurai, "Effect of substitution of B-sites by Mn, Fe and Co in double perovskite-type $Ba_3CaNb_2O_9$ on structure and electrical properties," *RSC Advances*, **3**, 23824 (2013).
13. H. T. Handal and V. Thangadurai, "Electrochemical characterization of multi-element-doped ceria as potential anodes for SOFCs," *Solid State Ionics*, **262**, 359 (2014).
14. M. Chen, S. Paulson, V. Thangadurai, and V. Birss, "Sr-rich chromium ferrite as symmetrical solid oxide fuel cell electrodes," *J. Power Sources*, **236**, 68 (2013).
15. A. Buyukaksoy, V. Petrovsky, and F. Dogan, "Efficient cathodes for solid oxide fuel cells prepared by polymeric precursor infiltration," *J. Electrochem. Soc.*, **159**, B67 (2011).
16. P. Holtappels, J. Bradley, J. T. S. Irvine, A. Kaiser, and M. Mogensen, "Electrochemical characterization of ceramic SOFC anodes," *J. Electrochem. Soc.*, **148**, A923 (2001).
17. T.-S. Oh and S. M. Haile, "Electrochemical behavior of thin-film Sm-doped ceria: insights from the point-contact configuration," *Phys. Chem. Chem. Phys.*, **17**, 13501 (2015).
18. D. M. Bierschenk, J. M. Haag, K. R. Poeppelmeier, and S. A. Barnett, "Performance and stability of $LaSr_2Fe_2CrO_{9-\delta}$-based solid oxide fuel cell anodes in hydrogen and carbon monoxide," *J. Electrochem. Soc.*, **160**, F90 (2013).
19. S. B. Adler, J. A. Lane, and B. C. H. Steele, "Electrode kinetics of porous mixed-conducting oxygen electrodes," *J. Electrochem. Soc.*, **143**, 3554 (1996).
20. S. B. Adler, "Factors governing oxygen reduction in solid oxide fuel cell cathodes," *Chem. Rev.*, **104**, 4791 (2004).
21. M. Hrovat, A. Ahmed-Khanlou, Z. Samardzija, and J. Holc, "Interactions between lanthanum gallate based solid electrolyte and ceria," *Mater. Res. Bull.*, **34**, 2027 (1999).
22. K. Singh and V. Thangadurai, "Chemical reactivity between $Ce_{0.7}RE_{0.2}Mo_{0.1}O_2$ (RE=Y, Sm) and 8YSZ, and conductivity studies of their solid solutions," *Solid State Ionics*, **262**, 444 (2014).
23. W. C. Chueh, W. Lai, and S. M. Haile, "Electrochemical behavior of ceria with selected metal electrodes," *Solid State Ionics*, **179**, 1036 (2008).
24. C. Steven A. M. S. DeCaluwea and S. J. Gregory, "Experimental characterization of thin-film ceria solid oxide fuel cell anodes," *ECS Transactions*, **16**, 235 (2009).
25. P. Lohsoontorn, D. J. L. Brett, and N. P. Brandon, "Thermodynamic predictions of the impact of fuel composition on the propensity of sulfur to interact with Ni and ceria-based anodes for solid oxide fuel cells," *J. Power Sources*, **175**, 60 (2008).
26. S. Song, R. O. Fuentes, and R. T. Baker, "Nanoparticulate ceria-zirconia anode materials for intermediate temperature solid oxide fuel cells using hydrocarbon fuels," *J. Mater. Chem.*, **20**, 9760 (2010).
27. E. S. Putna, J. Stubenrauch, J. M. Vohs, and R. J. Gorte, "Ceria-based anodes for the direct oxidation of methane in solid oxide fuel cells," *Langmuir*, **11**, 4832 (1995).

Downloaded on 2016-08-30 to IP 136.159.160.69 address. Redistribution subject to ECS terms of use (see ecsdl.org/site/terms_use) unless CC License in place (see abstract).

28. E. C. C. D. Souza and R. Muccillo, "Properties and applications of perovskite proton conductors," *Mater. Res.*, **13**, 385 (2010).
29. H. T. Handal and V. Thangadurai, "Evaluation of chemical stability, thermal expansion coefficient, and electrical properties of solid state and wet-chemical synthesized Y and Mn-codoped CeO_2 for solid oxide fuel cells," *J. Power Sources*, **243**, 458 (2013).
30. M. Kobayashi and M. Flytzani-Stephanopoulos, "Reduction and sulfidation kinetics of cerium oxide and Cu-modified cerium oxide," *Ind. Eng. Chem. Res.* **41**, 3115 (2002).
31. M. A. Perrin and E. Wimmer, "Color of pure and alkali-doped cerium sulfide: A local-density-functional study," *Phys. Rev. B.*, **54**, 2428 (1996).
32. S. Zha, Z. Cheng, and M. Liu, "Sulfur poisoning and regeneration of Ni-based anodes in solid oxide fuel cells," *J. Electrochem. Soc.*, **154**, B201 (2007).
33. M. T. Hepworth, R. Ben-Slimane, and S. Zhong, "Thermodynamic comparison of several sorbent systems for hot coal-derived fuel-gas desulfurization," *Energy Fuels*, **7**, 602 (1993).
34. R. Ben-Slimane and M. T. Hepworth, "Desulfurization of hot coal-derived fuel gases with manganese-based regenerable sorbents. 1. loading (sulfidation) tests," *Energy Fuels*, **8**, 1175 (1994).
35. Z. Li and M. Flytzani-Stephanopoulos, "Cu−Cr−O and Cu−Ce−O regenerable oxide sorbents for hot gas desulfurization," *Ind. Eng. Chem. Res.*, **36**, 187 (1997).
36. H. H. M. Thi, B. Saubat, N. Sergent, and T. Pagnier, "In situ Raman and optical characterization of H_2S reaction with Ni-based anodes for SOFCs," *Solid State Ionics*, **272**, 84 (2015).
37. Z. Cheng, H. Abernathy, and M. Liu, "Raman spectroscopy of nickel sulfide Ni_3S_2," *J. Phys. Chem. C*, **111**, 17997 (2007).
38. A. O. Stormer, P. Holtappels, H. Y. Tu, and U. Stimming, "Electrochemical behavior of $Ce_{0.9}Gd_{0.1}O_{2-\delta}$ sofc-anodes," *Materialwiss. Werkstofftech.*, **33**, 339 (2002).
39. O. A. Marina and M. Mogensen, "High-temperature conversion of methane on a composite gadolinia-doped ceria–gold electrode," *Appl. Catal. A*, **189**,117 (1999).

Downloaded on 2016-08-30 to IP **136.159.160.69** address. Redistribution subject to ECS terms of use (see **ecsdl.org/site/terms_use**) unless CC License in place (see abstract).